


# Constraints on the nuclear equation of state and the neutron star structure from crustal torsional oscillations

Hajime Sotani<sup>1</sup> \*, Kei Iida<sup>2</sup>, and Kazuhiro Oyamatsu<sup>3</sup>

<sup>1</sup>*Division of Theoretical Astronomy, National Astronomical Observatory of Japan, 2-21-1 Osawa, Mitaka, Tokyo 181-8588, Japan*

<sup>2</sup>*Department of Mathematics and Physics, Kochi University, 2-5-1 Akebono-cho, Kochi 780-8520, Japan*

<sup>3</sup>*Department of Human Informatics, Aichi Shukutoku University, 2-9 Katahira, Nagakute, Aichi 480-1197, Japan*

7 December 2021

## ABSTRACT

We systematically examine torsional shear oscillations of neutron star crusts by newly taking into account the possible presence of the phase of cylindrical nuclei. In this study, we neglect an effect of magnetic fields, under which the shear oscillations can be damped by the magnetic interaction. First, by identifying the low frequency quasi-periodic oscillations (QPOs) observed in the soft-gamma repeaters (SGRs) as the fundamental torsional oscillations, we constrain the slope parameter of the nuclear symmetry energy,  $L$ , for reasonable values of the star’s mass  $M$  and radius  $R$ . Meanwhile, we find that the 1st overtone of torsional oscillations obtained for given  $M$  and  $R$  can be expressed well as a function of a new parameter  $\zeta \equiv (K_0^4 L^5)^{1/9}$ , where  $K_0$  is the incompressibility of symmetric nuclear matter. Assuming that the lowest of the QPO frequencies above 500 Hz observed in SGR 1806–20 comes from the 1st overtone, we can constrain the value of  $\zeta$ . Then, for each neutron star model, such a value of  $L$  as can be obtained from the observed low frequency QPOs translates to the optimal value of  $K_0$  via the above constraint on  $\zeta$ . Finally, its consistency with allowed values of  $K_0$  from empirical giant monopole resonances leads to neutron star models with relatively low mass and large radius, which are qualitatively similar to the prediction in earlier investigations. This result suggests that  $L \simeq 58\text{--}73$  MeV, even when uncertainties in the neutron superfluid density inside the phase of cylindrical nuclei are allowed for.

**Key words:** stars: neutron – equation of state – stars: oscillations

## 1 INTRODUCTION

Neutron stars, which are produced as stellar remnants of collapse of massive stars, exhibit states of matter in extreme conditions where the density inside the star exceeds the normal nuclear density significantly under the strong gravitational field, and the magnetic field inside/around the star can become extremely strong (Haensel, Potekhin & Yakovlev 2007). To extract the neutron star properties, asteroseismology is a powerful tool, just like seismology in the case of the Earth and helioseismology in the case of the Sun. That is, by observing the spectra of electromagnetic waves and/or gravitational waves radiating from the objects, one would see the interior properties of the objects. In fact, various eigenmodes could be excited in a neutron star in a manner that reflects the star’s mass  $M$  and radius  $R$ , the internal crystalline and superfluid properties, etc. (Van Horn et al. 1995). For example, via the observations of gravitational waves, one would constrain  $M$ ,  $R$ , and the equation of state (EOS) of neutron star matter (Andersson & Kokkotas 1996; Sotani, Tominaga & Maeda 2001; Sotani, Kohri & Harada 2004; Sotani et al. 2011; Doneva et al. 2013).

Theoretically, the structure of a neutron star strongly depends on the uncertain EOS for neutron star matter, while the qualitative structure with the canonical mass of order  $1.4M_\odot$  is fairly well established. In equilibrium, under the ocean composed of melted iron, the matter forms a lattice structure due to the Coulomb interaction and behaves as a solid. This

\* E-mail: sotani@yukawa.kyoto-u.ac.jp

region is referred to as a crust. As the density increases, the energy of matter in the lattice structure becomes larger than that of uniform matter. Above such a critical density, the neutron star matter becomes uniform and behaves as a fluid. This region is referred to as a core. The critical density is predicted to lie roughly between the normal nuclear density and one third thereof in a manner that is dependent on the density dependence of the symmetry energy (Oyamatsu & Iida 2007). Furthermore, the existence of the non-spherical nuclear structure has been proposed at the basis of the crust (Lorenz et al. 1993; Oyamatsu 1993), where the shape of non-spherical nuclei can change from spherical into cylindrical, slab-like, cylindrical-hole, and spherical-hole (bubble) nuclei, as the density increases. These phases of non-spherical nuclei are often called pasta phases. Anyway, the crust thickness is only less than ten per cent of  $R$ , determined mainly by the stellar compactness  $M/R$  and relatively weakly by such EOS parameters as the slope parameter of the nuclear symmetry energy  $L$  and the incompressibility of symmetric nuclear matter  $K_0$  (Sotani, Iida & Oyamatsu 2017b).

As far as asteroseismology in neutron stars is concerned, gravitational waves would convey helpful information, which is expected to be available in the near future. Meanwhile, electromagnetic signals from oscillating neutron stars have been already detected as quasi-periodic oscillations (QPOs) in the afterglow of giant flares observed from soft-gamma repeaters (SGRs). Up to now, at least three giant flares were detected from SGR 0526–66, SGR 1900+14, and SGR 1806–20, together with the associated QPOs (Barat et al. 1983; Israel et al. 2005; Strohmayer & Watts 2005, 2006). In particular, several QPOs were discovered at 28, 54, 84, and 155 Hz in SGR 1900+14 and at 18, 26, 29, 92.5, 150, 626.5, and 1837 Hz in SGR 1806–20. In addition to these QPOs observed in giant flares, a QPO of 57 Hz was also detected from SGR 1806–20 in less energetic bursts (Huppenkothen et al. 2014). Recently, the possible finding of QPOs of 9.2 Hz in SGR 1806–20 and 7.7 Hz in SGR 1900+14 has been also suggested with Bayesian analysis (Pumpe et al. 2018). Since SGRs are generally identified as strongly magnetized neutron stars, the observed QPOs are likely to be associated with the global oscillations. Such oscillations might be crustal torsional and/or magnetic oscillations, because the observed frequencies are relatively lower than typical  $p$ -mode oscillations of order kHz.

Up to now, many studies of magnetic and elasto-magnetic oscillations have been done by several groups (Sotani, Kokkotas & Stergioulas 2007, 2008a; Sotani, Colaiuda & Kokkotas 2008b; Sotani & Kokkotas 2009; van Hoven & Levin 2011, 2012; Colaiuda & Kokkotas 2011; Gabler et al. 2011, 2012, 2013a,b; Passamonti & Lander 2013). Given the magnetic field strength at the star’s surface estimated from the above SGRs (Kouveliotou et al. 1998; Hurley et al. 1999), the magnetic fields should penetrate the stellar core (Sotani, Colaiuda & Kokkotas 2008b). Then, the magnetic oscillations can be coupled with the crustal torsional oscillations, which are responsible for so-called elasto-magnetic oscillations. Details of this coupling strongly depend on the strength of magnetic fields. For example, the torsional oscillations would efficiently damp due to such coupling if the magnetic fields are stronger than  $\sim 5 \times 10^{13}$  G and dipolar (Gabler et al. 2011). Note, however, that the magnetic and elasto-magnetic oscillations are sensitive to the uncertain magnetic field strength and distribution inside the star. In addition, as long as the magnetic fields penetrate the stellar core, one requires information about the EOS of matter in the core, which is also uncertain, to construct the magnetic field structure<sup>1</sup>. On the other hand, if one neglects the magnetic effects, one can focus on torsional shear oscillations that are confined in the crust. Then, one can avoid uncertainties in the magnetic field structure and in the core EOS, while constructing a canonical model that can reproduce the observed QPO frequencies in a manner that is dependent on a limited number of parameters characterizing the neutron star structure and the properties of matter in the crust. Here we thus neglect the magnetic effects and focus on purely crustal torsional oscillations. In fact, assuming that the observed QPOs are identified as purely crustal torsional oscillations, one can constrain the EOS in the crust (Samuelsson & Andersson 2007; Steiner & Watts 2009; Gearheart et al. 2011; Passamonti & Andersson 2012; Sotani et al. 2012, 2013a,b). In addition, the QPOs could even give an imprint of the existence of pasta structures through the characteristic elastic properties (Sotani 2011; Passamonti & Pons 2016; Sotani, Iida & Oyamatsu 2017a).

Most of the calculations of the eigenfrequencies of crustal torsional oscillations, however, have been done by ignoring the possible presence of nuclear pasta. Since the thickness of the phases of non-spherical nuclei is at most about one per cent of  $R$  (Sotani, Iida & Oyamatsu 2017b), such ignorance is seemingly reasonable. In fact, the fundamental oscillations, of which the eigenfrequencies scale as the shear speed divided by  $2\pi R$ , are insensitive to the possible presence of nuclear pasta, although they are sensitive to  $L$  via the  $L$  dependence of the shear modulus (Sotani et al. 2012). On the other hand, the overtones, of which the eigenfrequencies scale as the shear speed divided by the crust thickness (Hansen & Cioffi 1980), are not necessarily so. Furthermore, the slab-like nuclear structure behaves like a fluid rather than a crystal against long wavelength linear perturbations (de Gennes & Prost 1993; Pethick & Potekhin 1998). Consequently, the crustal torsional oscillations can be separately excited inside the phases of spherical and cylindrical nuclei and inside the phases of cylindrical-hole and spherical-hole nuclei (Sotani, Iida & Oyamatsu 2017a). In this paper, we consider this possibility by newly examining the liquid-crystalline shear properties of cylindrical nuclei and then systematically calculating the fundamental and 1st overtone eigenfrequencies of the crustal torsional oscillations. By comparing the results with the observed QPO frequencies, we will

<sup>1</sup> There exists a recent attempt to constrain the EOS of matter in the core by comparing the elasto-magnetic oscillations to the observed QPO frequencies (Gabler et al. 2018).

be able to constrain not only  $M$  and  $R$ , but also  $L$ , in a manner that is almost independent of the poorly known neutron superfluid density inside the phase of cylindrical nuclei.

In Sec. 2, we construct the equilibrium configuration of a neutron star crust. Section 3 is devoted to calculations of the shear modulus in the crust including the phase of cylindrical nuclei. In Sec. 4, we therefrom obtain the eigenfrequencies of torsional shear oscillations, which are then compared with the observed QPO frequencies. Concluding remarks are given in Sec. 5. We use units in which  $c = G = 1$ , where  $c$  and  $G$  denote the speed of light and the gravitational constant, respectively.

## 2 CRUST IN EQUILIBRIUM

It is generally accepted that the celestial objects, which are responsible for SGRs and associated giant flares, are strongly magnetized neutron stars, i.e., magnetars. Even so, since the magnetic energy is much smaller than the gravitational binding energy, one can neglect the contribution of the magnetic fields to the star's pressure and density profiles. The thermal energy can also be neglected in describing the star's structure. Additionally, the observed rotational period from SGRs is generally very large. As a reasonable model for the corresponding stars, therefore, we can safely consider a spherically symmetric neutron star, where the line element is given in spherical coordinates by

$$ds^2 = -e^{2\Phi(r)} dt^2 + e^{2\Lambda(r)} dr^2 + r^2 d\theta^2 + r^2 \sin^2 \theta d\phi^2. \quad (1)$$

Here, the metric function,  $\Lambda(r)$ , is directly associated with the mass function,  $m(r)$ , via  $e^{-2\Lambda} = 1 - 2m/r$ .

Now, neutron star models can be constructed by integrating the well-known Tolman-Oppenheimer-Volkoff (TOV) equations together with the zero-temperature EOS of matter in neutron stars. Due to only a limited number of experimental and observational constraints on the EOS of dense nuclear matter, the EOS of neutron star matter has yet to be determined although numerous EOS models have been proposed up to now. In particular, there are many uncertainties in the EOS of matter in the core, compared to that in the crust. To avoid such uncertainties in the core EOS, therefore, we focus only on the crust region, where the equilibrium model is constructed by integrating the TOV equations from the star's surface inward down to the bottom of the crust for a given set of  $M$  and  $R$  (Iida & Sato 1997). In order to construct the crust in equilibrium, one has to prepare the EOS of matter in the crust, which is assumed to be composed of a mixture of saturated nuclear matter (liquid) and pure neutron matter (gas) that is neutralized and beta equilibrated by a uniform gas of electrons. In particular, we adopt the phenomenological EOS of nuclear matter constructed in such a way as to reproduce empirical data for masses and charge radii of stable nuclei within the Thomas-Fermi approach (Oyamatsu & Iida 2003). By using the EOS of crustal matter obtained therefrom (Oyamatsu & Iida 2007) (hereafter referred to as the OI-EOS), we systematically examine the dependence of the frequencies of torsional oscillations on the EOS parameters.

In the vicinity of the saturation density of symmetric nuclear matter,  $n_0$ , the bulk energy per baryon of uniform nuclear matter at zero temperature can be expressed as a function of baryon number density,  $n_b$ , and neutron excess,  $\alpha$ , as

$$w = w_0 + \frac{K_0}{18n_0^2} (n_b - n_0)^2 + \left[ S_0 + \frac{L}{3n_0} (n_b - n_0) \right] \alpha^2, \quad (2)$$

where  $w_0$  and  $K_0$  denote the saturation energy and incompressibility of symmetric nuclear matter, corresponding to  $\alpha = 0$  (Lattimer 1981). Meanwhile, the coefficients affixed to the term of order  $\alpha^2$ , i.e.,  $S_0$  and  $L$ , are the parameters associated with the density-dependent symmetry energy  $S(n_b)$ . That is,  $S_0$  is the symmetry energy at  $n_b = n_0$ , i.e.,  $S_0 = S(n_0)$ , while  $L$  is the slope parameter given by  $L \equiv 3n_0(dS/dn_b)_{n_b=n_0}$ . These five parameters,  $n_0$ ,  $w_0$ ,  $K_0$ ,  $S_0$ , and  $L$  are the parameters that characterize the properties of nuclear matter around the saturation point. Through terrestrial nuclear experiments, whose data basically reflect the properties of saturated nuclear matter that has a limited range of neutron excess, these parameters can be more or less constrained. Among them,  $n_0$ ,  $w_0$ , and  $S_0$  are relatively well-constrained, while the other two parameters,  $K_0$  and  $L$  are more difficult to determine. This is because one needs to obtain information for nuclear matter in a certain range of density around the saturation point to determine the values of  $K_0$  and  $L$ , which are higher order coefficients with respect to the change in density from  $n_0$ . Within the extended Thomas-Fermi theory incorporating the bulk energy expression that reduces to Eq. (2) in the limit of  $n_b \rightarrow n_0$  and  $\alpha \rightarrow 0$ , therefore, the OI-EOS was constructed by optimizing the values of  $n_0$ ,  $w_0$ , and  $S_0$  to reproduce experimental data for masses and charge radii of stable nuclei for given values of  $K_0$  and  $L$  (Oyamatsu & Iida 2007). The EOS parameter sets adopted in this study are shown in Table 1, together with the transition density from spherical nuclei to cylindrical nuclei and that from cylindrical nuclei to slab-like nuclei (or to uniform matter). Note that for  $L \gtrsim 100$  MeV, no pasta was predicted to occur.

For calculating the frequencies of torsional oscillations in the crust of a neutron star, one has to estimate the effective enthalpy density,  $\tilde{H}$ , that contributes to the oscillations. In fact, such frequencies are proportional to the shear speed defined as  $v_s = (\mu/\tilde{H})^{1/2}$  (Hansen & Cioffi 1980), where  $\mu$  denotes the shear modulus that will be described in the next section. The effective enthalpy density can be obtained by subtracting the mass density of superfluid neutrons from the total enthalpy density,  $H$ , in equilibrium. Since the baryon chemical potential is given by  $\mu_b = H/n_b$  at zero temperature, the effective enthalpy density can be written as

**Table 1.** The EOS parameters adopted in this study and the corresponding transition density from spherical to cylindrical nuclei (SP–C) and that from cylindrical to slab-like nuclei (C–S). The asterisk at the value of  $K_0$  denotes the EOS model where cylindrical nuclei directly change to uniform matter.

$K_0$ (MeV)	$L$ (MeV)	$-y$ (MeV fm <sup>3</sup> )	SP–C (fm <sup>−3</sup> )	C–S (fm <sup>−3</sup> )
180	5.7	1800	0.06000	0.08665
180	31.0	350	0.05887	0.07629
180	52.2	220	0.06000	0.07186
230	7.6	1800	0.05816	0.08355
230	42.6	350	0.06238	0.07671
230	73.4	220	0.06421	0.07099
280	54.9	350	0.06638	0.07743
280*	97.5	220	0.06678	0.06887
360	12.8	1800	0.05777	0.08217
360	76.4	350	0.07239	0.07797

$$\tilde{H} = \left(1 - \frac{N_s}{A}\right) H, \quad (3)$$

where  $A$  is the baryon number in a Wigner-Seitz cell, while  $N_s$  is the number of neutrons in a Wigner-Seitz cell that do not comove with protons in the nuclei (Sotani et al. 2013a,b; Sotani, Iida & Oyamatsu 2017a).

Since we will confine ourselves to spherical and cylindrical nuclei in this work, we may assume that  $N_s$  comes solely from a part of the dripped neutron gas. Even under this assumption, it is uncertain how much fraction of dripped neutrons behave as a superfluid (Carter, Chamel & Haensel 2005; Chamel 2005, 2012; Watanabe & Pethick 2017). We thus introduce a new parameter  $N_s/N_d$  with the number of dripped neutrons in the Wigner-Seitz cell,  $N_d$ . Note that  $N_s/N_d = 0$  and 1 are the extreme cases, i.e., for  $N_s/N_d = 0$  all the dripped neutrons comove with the protons and  $\tilde{H}$  is equivalent to  $H$ , while for  $N_s/N_d = 1$  all the dripped neutrons behave as a superfluid and do not participate in the oscillations. The value of  $N_s/N_d$  in a realistic situation depends on the baryon density inside the star through the Bragg scattering of the dripped neutrons off the underlying crystalline structure. In practice,  $N_s/N_d$  in the phase of spherical nuclei becomes around 10–30 per cent for  $n_b \sim 0.01\text{--}0.4n_0$ , according to band calculations that ignore the effect of nonzero pairing gap (Chamel 2012). On the other hand,  $N_s/N_d$  in the phase of cylindrical nuclei is more uncertain and more complicated, because the entrainment in this layer would be anisotropic with respect to the orientation of cylindrical nuclei. To obtain the isotropic effective mass of dripped neutrons, it is often assumed that the polycrystalline orientation of cylindrical nuclei is random. Here again, according to the band calculations by Chamel (2005); Carter, Chamel & Haensel (2005) in the absence of the effect of nonzero pairing gap, the isotropic effective mass becomes  $m_*/m = 1.185$  at the  $n_b = 0.06 \text{ fm}^{-3}$ , which corresponds to  $N_s/N_d$  of 84.4 per cent. This may suggest that as compared to the phase of spherical nuclei, a much greater part of the dripped neutrons behave as a superfluid. The effect of nonzero pairing gap, however, acts to reduce entrainment due to the band effect in a manner that is dependent on the ratio of the pairing and band gaps and on the dimension of the crystalline structure (Watanabe & Pethick 2017). In the present analysis, for simplicity, we set  $N_s/N_d$  in the phase of spherical nuclei to the results obtained by Chamel (2012), as in Sotani et al. (2013a,b), while we consider  $N_s/N_d$  in the phase of cylindrical nuclei as a free parameter that ranges  $0 \leq N_s/N_d \leq 1$ . In particular, we will consider the extreme cases, i.e.,  $N_s/N_d = 0$  and 1 in the phase of cylindrical nuclei. To describe crustal torsional oscillations, therefore, we have to set the values of two stellar parameters, i.e.,  $M$  and  $R$ , two EOS parameters, i.e.,  $L$  and  $K_0$ , and  $N_s/N_d$  in the phase of cylindrical nuclei.

### 3 SHEAR MODULUS

The shear modulus is another important parameter for description of the crustal torsional oscillations. For a bcc lattice of spherical nuclei the effective shear modulus has been derived as

$$\mu_{\text{sp}} = 0.1194 \frac{n_i (Ze)^2}{a}, \quad (4)$$

where  $n_i$  is the number density of nuclei with the charge number of  $Z$ , and  $a$  is the radius of the Wigner-Seitz cell, i.e.,  $1/n_i = 4\pi a^3/3$  (Ogata & Ichimaru 1990; Strohmayer et al. 1991). We remark that this shear modulus was derived by assuming that each nucleus is a point particle and by taking average over all possible wave vectors of displacements in such a way as to be relevant for polycrystalline matter with randomly oriented crystallites. In the present analysis we simply adopt this traditional formula for the shear modulus in the phase of spherical nuclei, although modified versions of the shear modulus that allow for electron screening and more realistic but still randomly oriented polycrystalline nature (Kobyakov & Pethick 2013, 2015) are also proposed. These modifications could act to reduce the effective shear modulus roughly by 30 per cent,

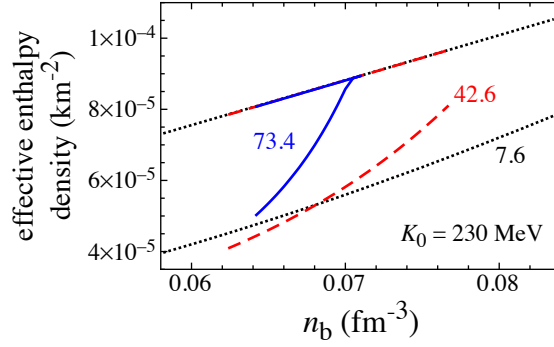


**Figure 1.** Effective enthalpy density ( $\tilde{H}$ ) in the phase of cylindrical nuclei. The dotted, dashed, and solid lines correspond to the results obtained for  $L = 7.6, 42.6,$  and  $73.4$  MeV, respectively, by fixing the value of  $K_0$  to 230 MeV. For each EOS model, the upper and lower lines denote the effective enthalpy with  $N_s/N_d = 0$  and 1.

while the effect of nonzero pairing gap could lead to reduction of the effective enthalpy density by the same order or even larger than that (Watanabe & Pethick 2017). Fortunately, these two uncertain factors would counteract with each other in evaluations of the torsional oscillation frequencies, but eventually, full account of these factors would be desired.

Let us now move on to the shear modulus in the phase of cylindrical nuclei. In this region, the equilibrium configuration of cylindrical nuclei is likely to be a two-dimensional triangular lattice. According to de Gennes & Prost (1993); Pethick & Potekhin (1998), who assumed that the direction of cylindrical axes is locally  $z$ -direction and that the two-dimensional displacement of  $(u^x, u^y)$  arises on the plane normal to the  $z$ -direction, the energy due to the deformation,  $E_d$ , is given by

$$\begin{aligned}
 E_d = & \frac{B_1}{2} \left( \frac{\partial u^x}{\partial x} + \frac{\partial u^y}{\partial y} \right)^2 + \frac{C}{2} \left[ \left( \frac{\partial u^x}{\partial x} - \frac{\partial u^y}{\partial y} \right)^2 + \left( \frac{\partial u^x}{\partial y} + \frac{\partial u^y}{\partial x} \right)^2 \right] + \frac{K_3}{2} \left[ \left( \frac{\partial^2 u^x}{\partial z^2} \right)^2 + \left( \frac{\partial^2 u^y}{\partial z^2} \right)^2 \right] \\
 & + B_2 \left( \frac{\partial u^x}{\partial x} + \frac{\partial u^y}{\partial y} \right) \left[ \left( \frac{\partial u^x}{\partial z} \right)^2 + \left( \frac{\partial u^y}{\partial z} \right)^2 \right] + \frac{B_3}{2} \left[ \left( \frac{\partial u^x}{\partial z} \right)^2 + \left( \frac{\partial u^y}{\partial z} \right)^2 \right]^2, \quad (5)
 \end{aligned}$$

where the terms with  $B_1$ ,  $C$ , and  $K_3$  are associated with the uniform transverse compression or dilation, transverse shear, and bending, respectively. On the other hand, the terms with  $B_2$  and  $B_3$  are higher-order terms with respect to the displacement of  $(u^x, u^y)$ , which are negligible in the linear analysis as adopted here. For the torsional oscillations, therefore, only the coefficient  $C$  is relevant and acts as a shear modulus.

In order to estimate the value of  $C$ , one should calculate the change of energy by imposing an appropriate perturbation for transverse shear. In this case,  $E_d$  corresponds to the change in the Coulomb energy due to transverse shear that does not involve deformation of the cross section of each cylinder. Let us now set the Coulomb energy per unit volume,  $E_{\text{Coul}}$ , for the equilibrium phase of cylindrical nuclei. By calculating the spacially averaged Coulomb energy per unit volume,  $\langle E_{\text{Coul}} \rangle$ , in the presence of the above perturbation with respect to the displacement of  $(u^x, u^y)$  and by identifying  $E_d$  with  $\langle E_{\text{Coul}} \rangle - E_{\text{Coul}}$ , one can estimate the value of  $C$ . In practice,  $C$  has been approximately estimated as

$$C = E_{\text{Coul}} \times 10^{2.1(w_2 - 0.3)}, \quad (6)$$

for a relevant range of the volume fraction,  $w_2$ , occupied by cylindrical nuclei (Pethick & Potekhin 1998), where  $w_2$  is defined as  $w_2 \equiv (R_p/R_c)^2$  with the radius of the cross section of a cylindrical nucleus  $R_p$  and the corresponding Wigner-Seitz radius  $R_c$ . In addition, given polycrystalline matter with randomly oriented crystallites as in the case of spherical nuclei<sup>2</sup>, average of  $C$  over all possible wave vectors of displacements leads to an effective shear modulus,  $\mu_{\text{cy}}$ , as

$$\mu_{\text{cy}} = \frac{2}{3}C. \quad (7)$$

In the present analysis, we adopt this type of shear modulus in the phase of cylindrical nuclei for calculations of the eigenfrequencies of torsional oscillations. To estimate the effective shear modulus  $\mu_{\text{cy}}$  at given baryon density, we utilize the corresponding value of  $E_{\text{Coul}}$  that was obtained when the OI-EOS was constructed within the Thomas-Fermi model. We remark that in the liquid drop model  $E_{\text{Coul}}$  is given by

$$E_{\text{Coul}} = \frac{\pi}{2} (\rho_p R_p)^2 w_2 \left[ \ln \left( \frac{1}{w_2} \right) - 1 + w_2 \right], \quad (8)$$

<sup>2</sup> Orientations of crystallites might be affected not only by gravitational and magnetic fields, but also by inhomogeneities in the local environment prior to nucleation. In this study, however, we simply consider the case of randomly oriented crystallites.



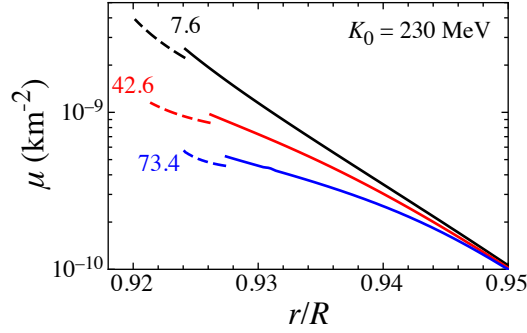


**Figure 2.** Effective shear modulus in the phase of spherical nuclei ( $\mu_{\text{sp}}$ ) and in the phase of cylindrical nuclei ( $\mu_{\text{cy}}$ ), plotted by the solid and dashed lines, respectively, for stellar models with  $1.4M_{\odot}$  and 12 km. Each line corresponds to the case of  $L = 7.6, 42.6,$  and  $73.4$  MeV from top to bottom, where the value of  $K_0$  is fixed to 230 MeV.

where  $\rho_p$  is the charge density in a cylindrical liquid drop, i.e.,  $\rho_p \equiv en_p$  with the local proton number density,  $n_p$  (Ravenhall, Pethick & Wilson 1983).

Additionally, the phase of slab-like nuclei is predicted to occur just below the phase of cylindrical nuclei in a manner that is dependent on the EOS parameters. The elastic properties in the phase of slab-like nuclei have been also discussed in de Gennes & Prost (1993); Pethick & Potekhin (1998), where they showed that the energy-change due to the deformation is of higher order in the displacement. That is, the phase of slab-like nuclei behaves as a fluid for long-wavelength torsional motion as can be examined in the linear analysis. Even if additional pasta phases occur just below the phase of slab-like nuclei, therefore, the torsional oscillations are confined in the region of spherical and cylindrical nuclei, which can be analyzed independently of the torsional oscillations in the region of cylindrical-hole and spherical-hole nuclei (Sotani, Iida & Oyamatsu 2017a).

For this reason, we can focus on the oscillations that are confined to the region of spherical and cylindrical nuclei, where the corresponding effective shear modulus is given by  $\mu_{\text{sp}}$ , Eq. (4), and  $\mu_{\text{cy}}$ , Eq. (7), respectively. In Fig. 2, we show the radial dependence of the effective shear modulus in the region of spherical and cylindrical nuclei for the stellar model with  $1.4M_{\odot}$  and 12 km, which is obtained for three sets of the EOS parameters. We remark that the shear modulus would be graphically the same among the three cases if extended up to the star's surface. From this figure, one can observe that the effective shear modulus decreases discontinuously at the transition point from spherical nuclei to cylindrical nuclei. This is due to the sudden change of the crystalline structure (Araki 2014).

#### 4 TORSIONAL OSCILLATIONS AND COMPARISON WITH OBSERVED QPOS

In order to determine the frequencies of torsional oscillations in the crust of a spherical neutron star, we consider a linear analysis on the star's equilibrium configuration. Since the torsional oscillations are of axial type and hence do not involve density variations, we can safely adopt the relativistic Cowing approximation in which the metric perturbations are neglected. Owing to the spherically symmetric background, the oscillations are described by one perturbation variable, i.e., the Lagrangian displacement ( $\mathcal{Y}$ ) of a given matter element in the  $\phi$  direction. The differential equation obeyed by this variable can be derived by linearizing the relativistic equation of motion as

$$\mathcal{Y}'' + \left[ \left( \frac{4}{r} + \Phi' - \Lambda' \right) + \frac{\mu'}{\mu} \right] \mathcal{Y}' + \left[ \frac{\tilde{H}}{\mu} \omega^2 e^{-2\Phi} - \frac{(\ell+2)(\ell-1)}{r^2} \right] e^{2\Lambda} \mathcal{Y} = 0, \quad (9)$$

where  $\tilde{H}$  is the effective enthalpy given in section 2, the prime denotes the differentiation with respect to  $r$ , and  $\omega$  denotes the angular frequency of torsional oscillations, of which the value will be determined from boundary conditions to be specified below (Schumaker & Thorne 1983). We notice that  $\omega$  is associated with the frequency  $f$  of torsional oscillations via  $\omega = 2\pi f$ . Since we consider the eigenmodes of torsional oscillations inside the phases of spherical and cylindrical nuclei in the present analysis, we impose relevant boundary conditions: At the star's surface, the torque vanishes, while at the base of the phase of cylindrical nuclei, the traction force vanishes. Both conditions can be expressed as  $\mathcal{Y}' = 0$  (Schumaker & Thorne 1983; Sotani, Kokkotas & Stergioulas 2007). Additionally, we impose a junction condition at the interface between the phase of spherical nuclei and the phase of cylindrical nuclei, which has to be a continuous traction condition, i.e.,

$$\mu_{\text{sp}} \mathcal{Y}' = \mu_{\text{cy}} \mathcal{Y}'. \quad (10)$$

Furthermore, since we can choose an arbitrary amplitude of torsional oscillations in Eq. (9), we adopt the amplitude at the star's surface as a unit length. Then, the problem to solve becomes an eigenvalue problem with respect to  $\omega$ . Hereafter, we

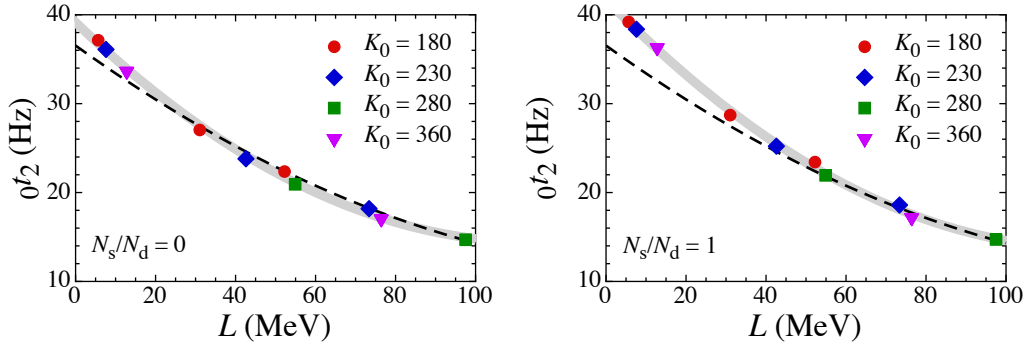


**Figure 3.** The fundamental frequencies  ${}_0t_2$  of the  $\ell = 2$  torsional oscillations globally excited in the phases of spherical and cylindrical nuclei, which are calculated for various EOS models and for stellar models with  $M = 1.4M_\odot$  and  $R = 12$  km. The results are plotted in symbols as a function of  $L$  in the case of  $N_s/N_d = 0$  (left) and  $N_s/N_d = 1$  (right) in the phase of cylindrical nuclei. In both panels, the thick solid line denotes the fitting formula given by Eq. (11), while the dashed line denotes the same kind of formula for the oscillations not involving the phase of cylindrical nuclei.

use the notation,  ${}_nt_\ell$ , in expressing the torsional eigenfrequencies with the angular index  $\ell$  and the number  $n$  of radial nodes in the eigenfunction.

#### 4.1 Fundamental oscillations

First, we examine the fundamental frequencies of torsional oscillations, i.e.,  ${}_0t_\ell$ , in a manner that is dependent on the EOS parameters  $L$  and  $K_0$ . A similar analysis for the fundamental crustal torsional oscillations confined in the phase of spherical nuclei has been already done (Sotani et al. 2012, 2013a,b; Sotani 2014; Sotani, Iida & Oyamatsu 2016; Sotani 2016), where it was shown that the fundamental frequencies of torsional oscillations are almost independent of the value of  $K_0$ . In the presence of cylindrical nuclei, however, the earlier calculations are not always realistic because the cylindrical phase has nonzero shear modulus as shown in Fig. 2. Now, we thus calculate the  $\ell = 2$  fundamental frequencies of torsional oscillations that are globally excited in the phases of spherical and cylindrical nuclei. The resultant frequencies, which are obtained for stellar models with  $M = 1.4M_\odot$  and  $R = 12$  km, various EOS models shown in Table 1, and  $N_s/N_d = 0, 1$  in the phase of cylindrical nuclei, are exhibited in Fig. 3. From this figure, we can confirm that the  $\ell = 2$  fundamental frequencies of oscillations involving the phase of cylindrical nuclei are still almost independent of the value of  $K_0$ . In practice, we find that the dependence of the  $\ell = 2$  fundamental frequencies on  $L$  can be expressed as

$${}_0t_2 = c_2^{(0)} + c_2^{(1)}L + c_2^{(2)}L^2, \quad (11)$$

where  $c_2^{(0)}$ ,  $c_2^{(1)}$ , and  $c_2^{(2)}$  are coefficients that are determined by a fit to the calculations of  ${}_0t_2$  for various  $L$ . The values from this fitting formula are also plotted in Fig. 3, together with those from the same kind of fitting formula for the oscillations confined in the phase of spherical nuclei. By comparing these two cases, we find that the effect of the phase of cylindrical nuclei is generally small and acts to increase the fundamental frequencies of torsional oscillations only for small values of  $L$  for which the phase of cylindrical nuclei is predicted to have a relatively large density range as shown in Table 1.

In addition, we similarly calculate the  $\ell$ -th order fundamental frequencies of torsional oscillations,  ${}_0t_\ell$ , from various EOS models and find that the dependence of  ${}_0t_\ell$  on  $K_0$  is negligible for neutron star models ranging  $M = 1.4$ – $1.8M_\odot$  and  $R = 10$ – $14$  km. Thus, one can generally express  ${}_0t_\ell$  as a function of  $L$  as

$${}_0t_\ell = c_\ell^{(0)} + c_\ell^{(1)}L + c_\ell^{(2)}L^2, \quad (12)$$

where  $c_\ell^{(0)}$ ,  $c_\ell^{(1)}$ , and  $c_\ell^{(2)}$  are coefficients that can be determined from fitting to the calculations of  ${}_0t_\ell$  as a function of the star's mass and radius.

Let us proceed to constrain the value of  $L$  by comparing the  $\ell = 2$  fundamental frequencies of crustal torsional oscillations with the lowest QPO frequency observed in giant flares. In Fig. 4, the prediction of  ${}_0t_2$  is shown for stellar models with  $M = 1.4$ – $1.8M_\odot$  and  $R = 10$ – $14$  km in the case of  $N_s/N_d = 0$  and 1 in the phase of cylindrical phase. Note that  ${}_0t_2$  is the lowest frequency among the torsional oscillations. Given our interpretation of the QPO frequencies in terms of crustal torsional oscillations, the lowest QPO frequency, i.e., 18 Hz, in SGR 1806–20 has to be higher than  ${}_0t_2$ . We thus obtain a constraint of  $L$  as  $L \gtrsim 51.9$  MeV for  $N_s/N_d = 0$  and  $L \gtrsim 56.1$  MeV for  $N_s/N_d = 1$ .

One may further constrain the value of  $L$  by identifying the observed QPOs as manifestations of various crustal torsional oscillations. In fact, we have shown the possibility of constraining  $L$  by fitting the calculated fundamental torsional oscillations with various  $\ell$  to the observed QPO frequencies lower than 100 Hz in our earlier investigations, where we neglected the effect

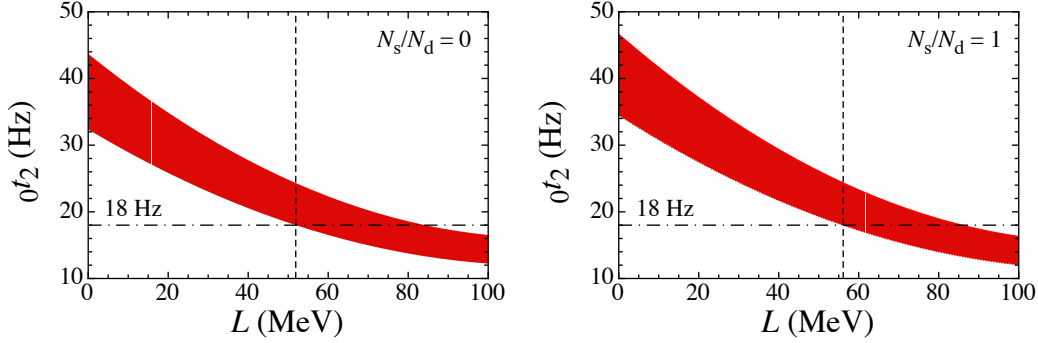


**Figure 4.** The  $L$  dependence of the eigenfrequency  ${}_0t_2$  calculated for stellar models with  $10 \leq R \leq 14$  km and  $1.4 \leq M/M_\odot \leq 1.8$  in the case of  $N_s/N_d = 0$  (left panel) and 1 (right panel) in the phase of cylindrical nuclei. The horizontal dot-dashed line denotes the lowest frequency observed in the giant flare observed from SGR 1806–20, while the vertical dashed line corresponds to  $L = 51.9$  MeV (left panel) and 56.1 MeV (right panel).

of the phase of cylindrical nuclei (Sotani et al. 2013a,b; Sotani, Iida & Oyamatsu 2016). In such an attempt, we found two possibilities of explaining the observed low frequency QPOs in terms of the crustal torsional oscillations, i.e., (i) 18, 26, 29, 57, and 92.5 Hz in SGR 1806–20 correspond to the  $\ell = 3, 4, 5, 9,$  and 15 fundamental torsional oscillations, and 28, 54, and 84 Hz in SGR 1900+14 correspond to the  $\ell = 4, 8,$  and 13 fundamental torsional oscillations. (ii) 18, 29, 57, and 92.5 Hz in SGR 1806–20 correspond to the  $\ell = 2, 3, 6,$  and 10 fundamental torsional oscillations, and 28, 54, and 84 Hz in SGR 1900+14 correspond to the  $\ell = 3, 6,$  and 9 fundamental torsional oscillations<sup>3</sup>. As for the first possibility, one can explain all the observed low frequency QPOs in terms of the crustal torsional oscillations, where the optimal value of  $L$  becomes larger than 100 MeV (Sotani et al. 2013a), but this constraint seems too large to be consistent with existing nuclear experiments, which implies typically  $L = 30\text{--}80$  MeV (Tsang et al. 2012; Lattimer 2014; Newton et al. 2014; Baldo & Burgio 2016). Meanwhile, the constraint on  $L$  resulting from the second possibility is more or less consistent with the experiments, although one has to invoke an additional oscillation mechanism for explaining the unidentified 26 Hz QPO. As a possible mechanism for that, we proposed torsional oscillations excited in the phase of bubble nuclei (Sotani, Iida & Oyamatsu 2017a); strictly speaking, these torsional oscillations, if occurring, would extend to the phase of cylindrical-hole nuclei, but would not affect the torsional oscillations in the phases of spherical and cylindrical nuclei because of vanishing shear modulus in the intervening phase of slab-like nuclei. Hereafter, we shall adopt the second possibility. In addition to the consistency with the empirical constraint on  $L$  as mentioned above, there are several reasons for that. One is that the two QPO frequencies, 26 and 29 Hz, are too close to make the first possibility satisfactory. Another is that the  $\ell = 2$  torsional oscillation frequency confined in the phases of bubble and cylindrical-hole nuclei can reproduce the 26 Hz QPO given uncertainty in the entrainment effect.

As shown in Fig. 5, the low frequency QPOs observed in SGR 1806–20 can in fact be explained in terms of the fundamental frequencies of crustal torsional oscillations with the specific values of  $\ell$  even by taking into account the presence of the phase of cylindrical nuclei. In particular, we find that the 150 Hz QPO can be explained in terms of the fundamental crustal torsional oscillations, simultaneously with the observed QPOs of frequencies lower than 100 Hz except the 26 Hz one; the corresponding  $\ell$  is 16. From this figure, the optimal value of  $L$  is found to be  $L = 73.4$  MeV for a typical neutron star model with  $M = 1.4M_\odot$  and  $R = 12$  km and with  $N_s/N_d = 1$  in the phase of cylindrical nuclei. Since the fundamental frequencies of the crustal torsional oscillations are predicted to decrease with  $M$  and  $R$ , the optimal value of  $L$  decreases with  $M$  and  $R$  as shown in Fig. 6, where the range of  $M = 1.4\text{--}1.8M_\odot$  and  $R = 10\text{--}14$  km and the value of  $N_s/N_d = 1$  in the phase of cylindrical nuclei are assumed. In this case, the optimal value of  $L$  turns out to be in the range of  $L = 55.7\text{--}85.1$  MeV.

In the same way, we find that the QPOs observed in SGR 1900+14 can be also identified as the fundamental crustal torsional oscillations, as shown in Fig. 7 for a typical neutron star model with  $M = 1.4M_\odot$ ,  $R = 12$  km, and  $N_s/N_d = 1$  in the phase of cylindrical nuclei. In particular, we find that the 155 Hz QPO can be identified as the  $\ell = 17$  fundamental crustal torsional oscillations, with the same accuracy as the identifications of the other QPO frequencies. In this case, the optimal value of  $L$  is  $L = 76.1$  MeV. Here again, the optimal value of  $L$  changes with  $M$  and  $R$  as shown in Fig. 8, where the range of  $M = 1.4\text{--}1.8M_\odot$  and  $R = 10\text{--}14$  km and the value of  $N_s/N_d = 1$  in the phase of cylindrical nuclei are assumed. From this figure, we find that the optimal value of  $L$  is in the range of  $L = 58.1\text{--}88.4$  MeV.

<sup>3</sup> In our previous studies where the effect of the phase of cylindrical nuclei was neglected, we adopted 30 Hz rather than 29 Hz as one of the observed QPO frequencies in SGR 1806–20. In fact, Israel et al. (2005) first reported the presence of the 30 Hz QPO. After that, however, Strohmayer & Watts (2006) concluded by reanalyzing the archival *RXTE* data that the QPO frequency is closer to 29 Hz than 30 Hz. In the present analysis, therefore, we adopt 29 Hz as the QPO frequency. As shown in text, 29 Hz is more preferable than 30 Hz in the second possibility of identifying the QPOs.



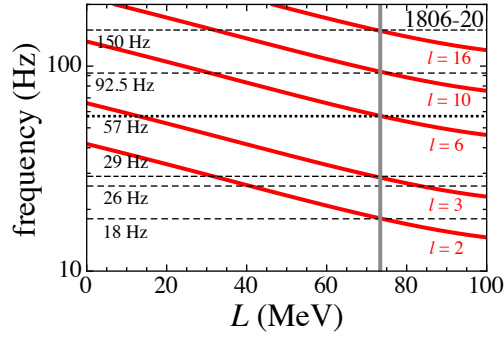


**Figure 5.** Comparison of the low-lying QPO frequencies observed in SGR 1806–20 (horizontal dashed and dotted lines) and the fundamental frequencies of crustal torsional oscillations (solid lines) obtained as a function of  $L$  for a neutron star model with  $M = 1.4M_{\odot}$ ,  $R = 12$  km, and  $N_s/N_d = 1$  in the phase of cylindrical nuclei. The vertical thick solid line denotes the optimal value of  $L$  that is consistent with the low frequency observed QPOs except the 26 Hz one.

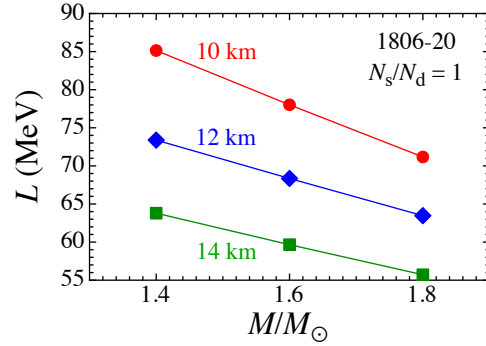


**Figure 6.** The optimal values of  $L$  that reproduce the low-lying QPO frequencies observed in SGR 1806–20 except 26 Hz in terms of the crustal torsional oscillations are plotted for various neutron star models with  $N_s/N_d = 1$  in the phase of cylindrical nuclei.

Since the value of  $L$  has to be uniquely determined, we can constrain the allowed values of  $L$  in such a way as to simultaneously explain the low frequency QPOs observed in SGR 1806–20 and in SGR 1900+14 in terms of the fundamental torsional oscillations in the crust of a neutron star of which the mass and radius is in the range of  $M = 1.4\text{--}1.8M_{\odot}$  and  $R = 10\text{--}14$  km. In the case of  $N_s/N_d = 1$  and 0 in the phase of cylindrical nuclei, as can be seen from Figs. 9 and 10, such constraint on  $L$  reads  $L = 58.1\text{--}85.1$  MeV and  $L = 53.9\text{--}83.6$  MeV, respectively. This suggests that uncertainty in  $N_s/N_d$  in the phase of cylindrical nuclei makes only a little difference in the constraint. In fact, even with such uncertainty taken into account, the allowed  $L$  lies in the range of  $L = 53.9\text{--}85.1$  MeV.

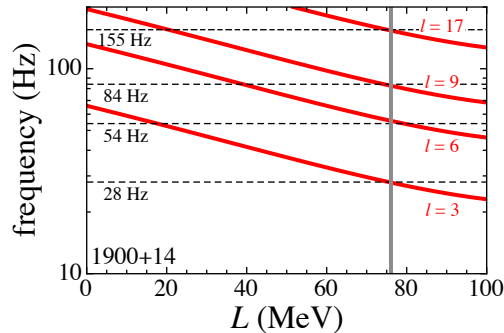


**Figure 7.** Same as Fig. 5, but for the QPO frequencies observed in SGR 1900+14.

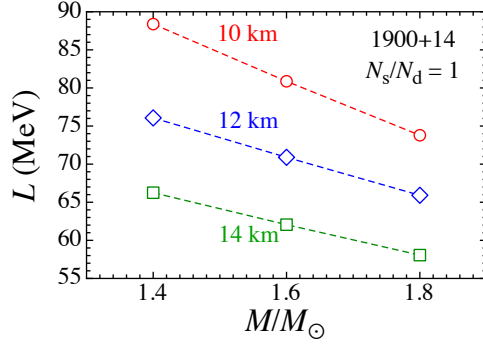


**Figure 8.** Same as Fig. 6, but for the low-lying QPO frequencies observed in SGR 1900+14.

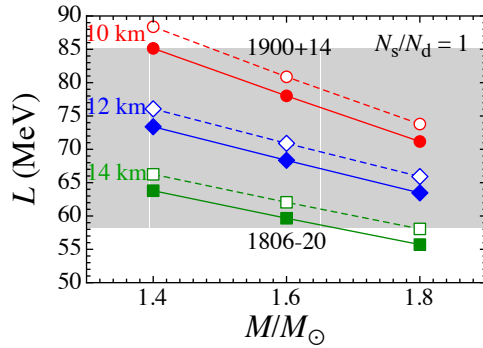


**Figure 9.** The values of  $L$  that simultaneously explain both of the low frequency QPOs observed in SGR 1806–20 (except the 26 Hz one) and SGR 1900+14 in terms of the fundamental torsional oscillations in the crust of a neutron star whose mass and radius range  $1.4\text{--}1.8M_\odot$  and  $10\text{--}14$  km. The painted region denotes such values of  $L$  in the case of  $N_s/N_d = 1$  in the phase of cylindrical nuclei, while the symbols denote the optimal values of  $L$  plotted in Figs. 6 and 8.

#### 4.2 The 1st overtones

Next, we turn to the properties of the 1st overtones of crustal torsional oscillations. Theoretically, the corresponding frequencies,  ${}_{1t_\ell}$ , are considered to be associated with the crust thickness,  $\Delta R$ , as  ${}_{1t_\ell} \propto v_s/\Delta R$  (Hansen & Cioffi 1980), whereas  $\Delta R$  in turn depends on the EOS parameters  $L$  and  $K_0$  mainly through the neutron chemical potential at the crust-core boundary (Sotani, Iida & Oyamatsu 2017b). Via identification of the relatively high frequency QPOs observed in SGR 1806–20 as the overtones of crustal torsional oscillations, therefore, one may obtain information about the EOS parameters (Sotani et al. 2012).

It is of great use to find a parameter that is constructed by a combination of  $K_0$  and  $L$  in such a way as to characterize the frequencies of the 1st overtones. To this end, let us consider the combination  $(K_0^i L^j)^{1/(i+j)}$  with integer numbers  $i$  and  $j$ . As a result of the parameter search, we find out a suitable combination, i.e.,

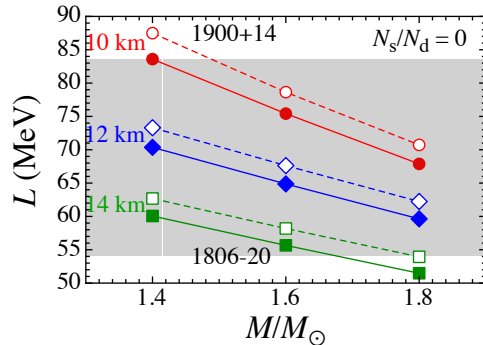


**Figure 10.** Same as Fig. 9, but with  $N_s/N_d = 0$  in the phase of cylindrical nuclei.

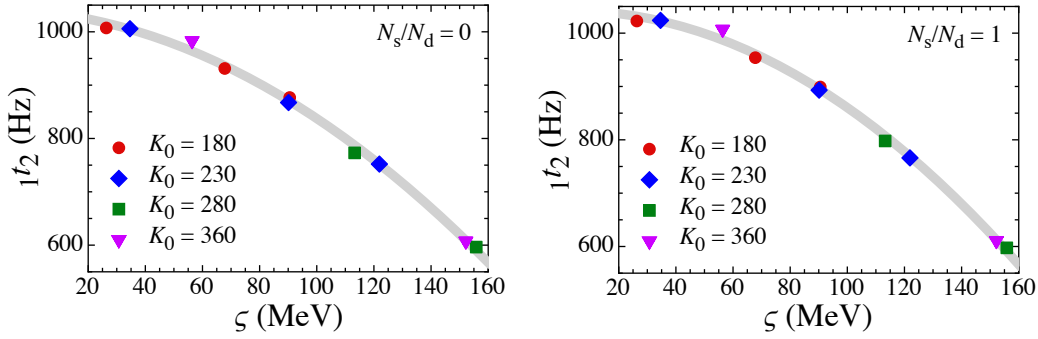


**Figure 11.** The 1st overtone frequencies of the  $\ell = 2$  torsional oscillations,  ${}_1t_2$ , calculated for various sets of the EOS parameters and for a neutron star model with  $M = 1.4M_\odot$  and  $R = 12$  km are plotted as a function of  $\zeta$  defined by Eq. (13). The left and right panels correspond to the results with  $N_s/N_d = 0$  and 1, respectively, in the phase of cylindrical nuclei. In both panels, the thick solid line denotes the fitting formula given by Eq. (14).

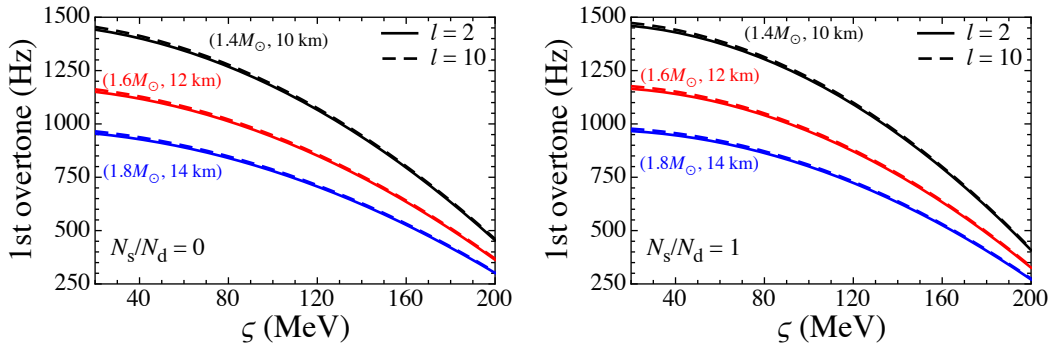


**Figure 12.** The 1st overtones of the  $\ell = 2$  (solid lines) and 10 (dashed lines) torsional oscillations are shown as a function of  $\zeta$  in the case of  $N_s/N_d = 0$  (left) and 1 (right) in the phase of cylindrical nuclei. In each panel, the lines from top to bottom correspond to the fitting formula [Eq. (15)] adjusted to the results obtained for neutron star models with  $(M, R) = (1.4M_\odot, 10$  km),  $(1.6M_\odot, 12$  km), and  $(1.8M_\odot, 14$  km).

$$\zeta = (K_0^4 L^5)^{1/9}. \quad (13)$$

We remark that the combination of  $K_0$  and  $L$  in  $\zeta$  is different from that in the parameter  $\eta$  defined by  $\eta = (K_0 L^2)^{1/3}$ , which is appropriate for describing the mass and radius of low-mass neutron stars (Sotani et al. 2014). In Fig. 11, the frequencies of the 1st overtones calculated for various EOS parameter sets are plotted as a function of  $\zeta$  by adopting a typical neutron star model with  $M = 1.4M_\odot$  and  $R = 12$  km and setting  $N_s/N_d = 0$  and 1 in the phase of cylindrical nuclei. From this figure, we find that the calculated frequencies behave smoothly as  $\zeta$  changes.

We can derive a fitting formula for the  $\ell = 2$  frequencies of the 1st overtones as the following quadratic function of  $\zeta$ :

$${}_1t_2 = d_2^{(0)} + d_2^{(1)}\zeta + d_2^{(2)}\zeta^2, \quad (14)$$

where  $d_2^{(0)}$ ,  $d_2^{(1)}$ , and  $d_2^{(2)}$  are adjustable coefficients that depend on  $M$  and  $R$ . Formula (14) well reproduces the calculated frequencies as shown in Fig. 11. Additionally, we can confirm that the  $\ell$ -th frequencies of the 1st overtones calculated for various neutrons star models can also be well reproduced by a quadratic function of  $\zeta$ ,

$${}_1t_\ell = d_\ell^{(0)} + d_\ell^{(1)}\zeta + d_\ell^{(2)}\zeta^2, \quad (15)$$

where  $d_\ell^{(0)}$ ,  $d_\ell^{(1)}$ , and  $d_\ell^{(2)}$  are adjustable coefficients that depend on  $M$  and  $R$ .

Unlike the fundamental frequencies of torsional oscillations, however, the overtone frequencies are closely spaced with respect to  $\ell$  (Hansen & Cioffi 1980), as is evident from comparison of the  $\ell = 2$  and 10 1st overtone frequencies in Fig. 12. Hereafter we thus focus only on the  $\ell = 2$  frequencies of the 1st overtones. Simultaneously, from this figure, one can observe that the frequencies of the 1st overtones strongly depend on the adopted neutron star models. This dependence, which occurs even with the compactness  $M/R$  almost fixed, reflect the fact that the crust thickness  $\Delta R$  scales as  $R$  for fixed compactness  $M/R$  (Sotani, Iida & Oyamatsu 2017b).

Now, we proceed to constrain  $\zeta$  by identifying the observed high frequency QPOs as the 1st overtones of crustal torsional oscillations. Although most of the QPOs observed in SGR 1806–20 and in SGR 1900+14 have a central frequency lower than

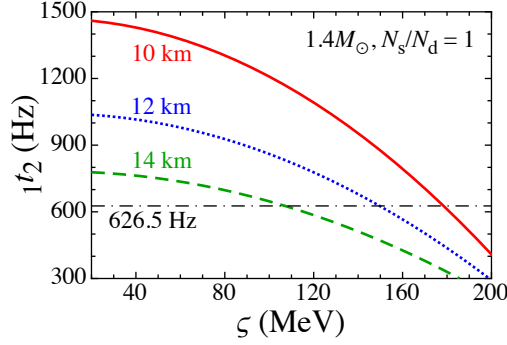


**Figure 13.** The fitting formula [Eq. (14)] adjusted to the calculations of  ${}_1t_2$  obtained for  $1.4M_\odot$  neutron stars of  $R = 10$  km (solid line), 12 km (dotted line), and 14 km (dashed line) in the case of  $N_s/N_d = 1$  in the phase of cylindrical nuclei. The 626.5 Hz QPO observed in SGR 1806–20 is also shown as dot-dashed line.

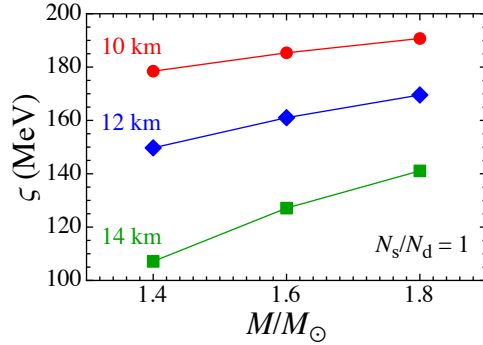


**Figure 14.** The optimal values of  $\zeta$  obtained in such a way as to explain the observed QPO 626.5 Hz in terms of  ${}_1t_2$  are plotted for various neutron star models with  $R = 10, 12, 14$  km,  $M = 1.4M_\odot, 1.6M_\odot, 1.8M_\odot$ , and  $N_s/N_d = 1$  in the phase of cylindrical nuclei.

160 Hz, the 626.5 and 1837 Hz QPOs are also observed in SGR 1806–20. Such high frequencies may come from something other than the torsional oscillations, e.g., polar type oscillations of neutron stars, but in the present study, we simply assume that the observed QPOs arise from purely crustal torsional oscillations. Then, it is reasonable to identify the 626.5 Hz QPO as the 1st overtone of crustal torsional oscillations of some  $\ell$ . By taking this identification for granted and by recalling that the calculated 1st overtone frequencies are closely spaced with respect to  $\ell$ , we can constrain the value of  $\zeta$  via comparison of the calculations of  ${}_1t_2$  with 626.5 Hz as shown in Fig. 13. From this figure, one can observe that the optimal values of  $\zeta$  are 178.5, 149.7, and 107.1 MeV for  $1.4M_\odot$  neutron stars of  $R = 10, 12$ , and 14 km, respectively, in the case of  $N_s/N_d = 1$  in the phase of cylindrical nuclei. In a similar way, the optimal values of  $\zeta$  can be obtained for various neutron star masses as shown in Fig. 14. We find that for each  $R$ , the optimal  $\zeta$  increases with  $M$ . This is because  $\Delta R$ , which typically behaves as  $\Delta R/R \simeq 2.1 \times 10^{-2}(R/M)(1 - 2M/R)$  (Sotani, Iida & Oyamatsu 2017b), decreases with the compactness  $M/R$ .

Once we obtain constraints on  $L$  and  $K_0$ , we can obtain information about  $M$  and  $R$  of the compact object associated with the QPOs. In fact, for each neutron star model, we can derive the optimal value of  $L$  in such a way as to explain the low-lying QPOs observed in SGR 1806–20 except the 26 Hz one as shown in Fig. 6 in the case of  $N_s/N_d = 1$  in the phase of cylindrical nuclei. By combining this  $L$  with the constraint on  $\zeta$  as shown in Fig. 14, we can then constrain  $K_0$  for each neutron star model via  $K_0 = (\zeta^9/L^5)^{1/4}$ . The resultant values of  $K_0$  are plotted in Fig. 15 with the filled marks and solid lines. On the other hand, the value of  $K_0$  is constrained from experiments on nuclear giant monopole resonances, e.g.,  $K_0 = 230 \pm 40$  MeV (Khan & Margueron 2013). We adopt this constraint on  $K_0$  as a typical one although it is still model dependent (see, e.g., Stone, Stone & Moszkowski (2014)). This constraint on  $K_0$ , which is also shown in Fig. 15, leads to  $M \simeq 1.4\text{--}1.5M_\odot$  for  $R = 14$  km, and presumably  $M \simeq 1.2\text{--}1.4M_\odot$  for  $R = 13$  km via extrapolations from the present calculations, as the favored neutron star models by the QPOs observed in SGR 1806–20 up to 626.5 Hz. This suggests that a compact object in SGR 1806–20 would have a relatively low mass and large radius. A similar result can also be obtained in the case of  $N_s/N_d = 0$  in the phase of cylindrical nuclei, as shown in Fig. 15 with the open marks and dashed lines. We remark in passing that a stellar model with still lower mass and smaller radius than that mentioned above might be acceptable judging from Fig. 15, but such a model would lead to a larger value of the optimal  $L$ , which in turn would be presumably inconsistent with the systematic analysis of the mass-radius relation of low-mass neutron stars (Sotani et al. 2014). We also remark that the same

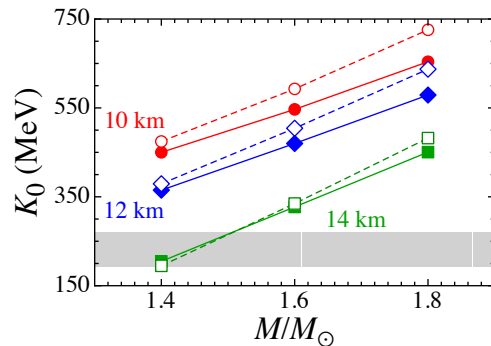


**Figure 15.** The constraint on  $K_0$  obtained by combining the constraints on  $L$  and  $\zeta$  from the observed QPOs in SGR 1806–20 is plotted for various neutron star models with  $N_s/N_d = 1$  (filled marks with solid lines) and  $N_s/N_d = 0$  (open marks with dashed lines) in the phase of cylindrical nuclei. The painted region denotes the empirical constraint on  $K_0$  (Khan & Margueron 2013).

kind of constraint on the neutron star model for SGR 1806–20 was obtained from a rather restricted set of the EOS models for neutron star matter (Deibel, Steiner & Brown 2014).

Given the present constraint on the neutron star model for SGR 1806–20, we can drastically improve the constraint on  $L$  over that shown in Figs. 9 and 10. In fact, the  $M$  and  $R$  constraint mentioned above leads to the favored values of  $L$  by the QPOs observed in SGR 1806–20 up to 626.5 Hz as roughly 62–73 (58–70) MeV for  $N_s/N_d = 1$  (0) in the phase of cylindrical nuclei. Within the uncertainty in this  $N_s/N_d$ , we can finally obtain  $L \simeq 58$ –73 MeV, which seems consistent with the existing empirical constraint on  $L$  (Tsang et al. 2012; Lattimer 2014; Newton et al. 2014; Baldo & Burgio 2016). For these favored  $L$  values, which are larger than 50 MeV, the pasta region is generally narrow. The cylindrical nuclei are thus expected to have only a little effect on the favored  $L$  values. In fact, the overtone frequencies  ${}_1t_2$  calculated by ignoring the presence of cylindrical nuclei (Sotani et al. 2012) are basically located between the present results obtained with  $N_s/N_d = 0$  and 1 in the phase of cylindrical nuclei. We remark that the 26 Hz QPO can be explained in terms of the torsional oscillations in the phases of cylindrical-hole and spherical-hole nuclei, as mentioned in the previous subsection, while the 1837 Hz QPO may well be explained in terms of the overtones of the crustal torsional oscillations of some specific  $n$  and  $\ell$ . On the other hand, if a possible new finding of the QPO of frequency less than 10 Hz pointed out by Pompe et al. (2018) is a true signal, the situation would become more complicated. In fact, the new candidate QPO frequency is too low to be identified in terms of purely crustal torsional oscillations. Then, one might have to consider an alternative oscillation mechanism such as magnetic oscillations.

## 5 CONCLUSION

We systematically calculate the fundamental and overtone eigenfrequencies of torsional oscillations that are excited in the crustal region composed of spherical and cylindrical nuclei by newly evaluating the shear modulus of the triangular lattice of cylindrical nuclei in such a way as to be consistent with the equilibrium configuration of neutron star matter obtained from various sets of the OI-EOS. As a first step to interpret the observed QPO frequencies, we focus on shear oscillations inside the crust. Despite the presence of the interaction of the shear oscillations with magnetic fields that penetrate the core, we prefer to neglect all related complications in this work and to improve on uncertainties associated with the calculations of purely crustal shear modes. In fact, the comprehensive study that includes uncertainties in the EOS parameters  $L$  and  $K_0$ , in the entrainment parameter  $N_s/N_d$  in the phase of cylindrical nuclei, and in the neutron star parameters  $M$  and  $R$  allows us to make a quantitative comparison between the calculated eigenfrequencies and the observed QPO frequencies. The resultant constraint on  $L$  from the low frequency QPO data is close to the previous constraint obtained by ignoring the effect of nonzero shear modulus of the phase of cylindrical nuclei, but leads to a constraint on  $M$  and  $R$  via the high frequency QPO data and the empirical constraint on  $K_0$ . This information on  $M$  and  $R$  helps us to further constrain  $L$  as  $\sim 58$ –73 MeV.

To make better estimates of the eigenfrequencies of crustal torsional oscillations, we will have to additionally consider shell and pairing effects on the charge number in the phase of spherical nuclei, the influence of nonzero pairing gap on the entrainment effect, and the question of how crustal polydispersity, magnetic fields, and plasticity affect the shear motion in a situation relevant for magnetars (Kobyakov & Pethick 2015; van Hoven & Levin 2011; Lander 2016). All these effects would definitely shift the pattern of the eigenfrequencies, leading to modification of the final constraint on  $L$ . Moreover, all we can mention about the 26 Hz QPO observed in SGR 1806–20 at present is the possibility that it arises from the fundamental  $\ell = 2$  torsional mode in the region composed of cylindrical-hole and spherical-hole nuclei. Whether or not this mode, if occurring in the deepest region of the crust, would be observable in the light curve has yet to be confirmed.



This work was supported in part by Grant-in-Aid for Scientific Research (C) through Grant No. 17K05458 provided by the Japan Society for the Promotion of Science (JSPS) and in part by Grant-in-Aid for Scientific Research on Innovative Areas through No. 24105008 provided by the Ministry of Education, Culture, Sports, Science and Technology of Japan (MEXT).

## REFERENCES

- Andersson N., Kokkotas K. D., 1996, *Phys. Rev. Lett.*, 77, 4134  
 Araki Y., 2014, Master thesis (in Japanese), Kochi University.  
 Baldo M., Burgio G. F., 2016, *Prog. Part. Nucl. Phys.*, 91, 203  
 Barat C. et al., 1983, *A&A*, 126, 400  
 Carter B., Chamel N., Haensel P., 2005, *Nucl. Phys. A*, 748, 675  
 Chamel N., 2005, *Nucl. Phys. A*, 747, 109  
 Chamel N., 2012, *Phys. Rev. C*, 85, 035801  
 Colaiuda A., Kokkotas K. D., 2011, *MNRAS*, 414, 3014  
 Deibel A. T., Steiner A. W., Brown E. F., 2014, *Phys. Rev. C*, 90, 025802  
 de Gennes P. G., Prost J., *The Physics of Liquid Crystals*, Oxford Univ. Press, Oxford  
 Doneva D. D., Gaertig E., Kokkotas K. D., Krüger C., 2013, *Phys. Rev. D*, 88, 044052  
 Gabler M., Cerdá-Durán P., Font J. A., Müller E., Stergioulas N., 2011, *MNRAS*, 410, L37  
 Gabler M., Cerdá-Durán P., Stergioulas N., Font J. A., Müller E., 2012, *MNRAS*, 421, 2054  
 Gabler M., Cerdá-Durán P., Font J. A., Müller E., Stergioulas N., 2013, *MNRAS*, 430, 1811  
 Gabler M., Cerdá-Durán P., Stergioulas N., Font J. A., Müller E., 2013, *Phys. Rev. Lett.*, 111, 211102  
 Gabler M., Cerdá-Durán P., Stergioulas N., Font J. A., Müller E., 2018, *MNRAS*, 476, 4199  
 Gearheart M., Newton W. G., Hooker J., Li B. A., 2011, *MNRAS*, 418, 2343  
 Hansen C., Cioffi D.F., 1980, *ApJ*, 238, 740  
 Haensel P., Potekhin A. Y., Yakovlev D. G., *Neutron Stars 1: Equation of State and Structure*, Springer, New York.  
 Huppenkothen D., Heil L. M., Watts A. L., Göğüş E., 2014, *ApJ*, 795, 114  
 Hurley K. et al., 1999, *Nature*, 397, L41  
 Iida K., Sato K., 1997, *ApJ*, 477, 294  
 Israel G. et al., 2005, *ApJ*, 628, L53  
 Khan E., Margueron J., 2013, *Phys. Rev. C*, 88, 034319  
 Kobayakov D., Pethick C. J., 2013, *Phys. Rev. C*, 87, 055803  
 Kobayakov D., Pethick C. J., 2015, *MNRAS*, 449, L110  
 Kouveliotou C. et al., 1998, *Nature*, 393, L235  
 Lander S. K., 2016, *ApJ*, 824, L21  
 Lattimer J. M., 1981, *Annu. Rev. Nucl. Part. Sci.*, 31, 337  
 Lattimer J. M., 2014, *Nucl. Phys. A*, 928, 276  
 Lorenz C. P., Ravenhall D. G., Pethick C. J., 1993, *Phys. Rev. Lett.*, 70, 379  
 Newton W. G., Hooker J., Gearheart M., Murphy K., Wen D. H., Fattoyev F. J., Li B. A., 2014, *Eur. Phys. J. A* 50, 41  
 Ogata S., Ichimaru S., 1990, *Phys. Rev. A*, 42, 4867  
 Oyamatsu K., 1993, *Nucl. Phys. A*, 561, 431  
 Oyamatsu K., Iida K., 2003, *Prog. Theor. Phys.*, 109, 631  
 Oyamatsu K., Iida K., 2007, *Phys. Rev. C*, 75, 015801  
 Passamonti A., Andersson N., 2012, *MNRAS*, 419, 638  
 Passamonti A., Lander S. K., 2013, *MNRAS*, 429, 767  
 Passamonti A., Pons J. A., 2016, *MNRAS*, 463, 1173  
 Pethick C. J., Potekhin A. Y., 1998, *Phys. Lett. B*, 427, 7  
 Pompe D., Gabler M., Steininger T., Enßlin T. A., 2018, *A&A*, 610, A61  
 Ravenhall D. G., Pethick C. J., Wilson J. R., 1983, *Phys. Rev. Lett.*, 50, 2066  
 Samuelsson L., Andersson N., 2007, *MNRAS*, 374, 256  
 Schumaker B. L., Thorne K. S., 1983, *MNRAS*, 203, 457  
 Sotani H., Tominaga K., Maeda K. I., 2001, *Phys. Rev. D*, 65, 024010  
 Sotani H., Kohri K., Harada T., 2004, *Phys. Rev. D*, 69, 084008  
 Sotani H., Kokkotas K. D., Stergioulas N., 2007, *MNRAS*, 375, 261  
 Sotani H., Kokkotas K. D., Stergioulas N., 2008a, *MNRAS*, 385, L5  
 Sotani H., Colaiuda A., Kokkotas K. D., 2008b, *MNRAS*, 385, 2161  
 Sotani H., Kokkotas K. D., 2009, *MNRAS*, 395, 1163

- Sotani H., 2011, MNRAS, 417, L70  
 Sotani H., Yasutake N., Maruyama T., Tatsumi T., 2011, Phys. Rev. D, 83, 024014  
 Sotani H., Nakazato K., Iida K., Oyamatsu K., 2012, Phys. Rev. Lett., 108, 201101  
 Sotani H., Nakazato K., Iida K., Oyamatsu K., 2013a, MNRAS, 428, L21  
 Sotani H., Nakazato K., Iida K., Oyamatsu K., 2013b, MNRAS, 434, 2060  
 Sotani H., 2014, Phys. Lett. B, 730, 166  
 Sotani H., Iida K., Oyamatsu K., Ohnishi A., 2014, Prog. Theor. Exp. Phys., 2014, 051E01  
 Sotani H., Iida K., Oyamatsu K., 2016, New Astron., 43, 80  
 Sotani H., 2016, Phys. Rev. D, 93, 044059  
 Sotani H., Iida K., Oyamatsu K., 2017a, MNRAS, 464, 3101  
 Sotani H., Iida K., Oyamatsu K., 2017b, MNRAS, 470, 4397  
 Steiner A. W., Watts A. L., 2009, Phys. Rev. Lett., 103, 181101  
 Strohmayer T., Van Horn H. M., Ogata S., Iyetomi H., Ichimaru S., 1991, ApJ., 375, 679  
 Strohmayer T. E., Watts A. L., 2005, ApJ, 632, L111  
 Strohmayer T. E., Watts A. L., 2006, ApJ, 653, 593  
 Stone J. R., Stone N. J., Moszkowski S. A., 2014, Phys. Rev. C, 89, 044316  
 Tsang M. B. *et al.*, 2012, Phys. Rev. C, 86, 015803  
 Van Horn H. M., Lee U., Epstein, R. I., Collins, T. J. B., in Ichimaru S., Ogata S., eds. Elementary Processes in Dense Plasmas, Addison-Wesley, Reading, p. 25  
 van Hoven M., Levin Y., 2011, MNRAS, 410, 1036  
 van Hoven M., Levin Y., 2012, MNRAS, 420, 3035  
 Watanabe G., Pethick C. J., 2017, Phys. Rev. Lett. 119, 062701